Publications of the Astronomical Society of Australia

An international journal of astronomy and astrophysics

www.publish.csiro.au/journals/pasa

Frequency Dependent Ray Paths in Local Helioseismology

G. Barnes[1,2] and P. S. Cally[2]

[1]High Altitude Observatory, National Center for Atmospheric Research,
Boulder CO 80307-3000, U.S.A. (current address)
barnesg@hao.ucar.edu
[2]Department of Mathematics & Statistics, P.O. Box 28M, Monash University, Vic 3800, Australia
paul.cally@sci.monash.edu.au

Abstract: The surface of the Sun is continually oscillating due to sound waves encroaching on it from the interior. Measurements of the surface velocity are used to infer some of the properties of the regions through which the sound waves have propagated. Traditionally, this has been done by using a modal decomposition of the surface disturbances. However, the use of ray descriptions, in the form of acoustic holography or time–distance helioseismology, provides an alternative approach which may reveal more detailed information about the properties of local phenomena such as sunspots and active regions. Fundamental to any such treatment is determining the correct ray paths in a given atmosphere. In the simplest approach, the ray paths are constructed to minimise the travel time between two points (Fermat's principle). However, such an approach is only valid in the high frequency limit, $\omega \gg \omega_c$, N, where ω_c is the acoustic cut-off and N the Brunt-Väisälä frequency. Although ω_c is often included in time–distance calculations, and N occasionally, the same is not true of acoustic holography. We argue that this raises concerns about image sharpness. As illustrations, representative ray paths are integrated in a realistic solar model to show that the Fermat approximation performs poorly for frequencies of helioseismic interest. We also briefly discuss the importance of the Brunt-Väisälä frequency to the time–distance diagram.

Keywords: Sun: oscillations — sunspots

1 Introduction

Acoustic waves propagate throughout the interior of the Sun. The conventional approach to analyzing these waves is through a modal decomposition (Deubner 1975; Unno et al. 1989). In this fashion, a great deal of information has been obtained regarding the internal structure of the Sun, including sound speed profile (Christensen-Dalsgaard et al. 1985), convection zone depth (Christensen-Dalsgaard, Gough & Thompson 1991), and differential rotation (see Hill, Deubner & Isaak 1991; Christensen-Dalsgaard & Berthomieu 1991; Charbonneau et al. 1998). In addition, local features, such as sunspots, have been probed. The modal method indicates that sunspots are strong absorbers of acoustic energy (Braun 1995), but gives little indication of their structure.

Two alternate approaches are time–distance helioseismology and acoustic holography. The former is explicitly founded on the ray or wave packet description rather than wave mechanics, and is generally formulated to account for dispersion, at least to the extent of retaining the acoustic cut-off frequency. The extent to which acoustic holography is either wave mechanical or ray theoretic is controversial and confusing, but Fermat's principle is clearly applied in the construction of its central diagnostic quantity, the acoustic egression (equation [2]; see also Lindsey & Braun 1997, §4.1), thereby ignoring dispersion. In this paper, we point out the potential significance of dispersion for the accurate holographic localisation of subsurface features.

1.1 Time–distance Helioseismology

Time–distance helioseismology (Duvall et al. 1993) utilises an approach commonly applied in both terrestrial and oceanographic seismology, extracting ray travel time information from cross-correlations of observed surface data. Specifically, letting $\Psi(\mathbf{x}, t)$ be a generic scalar representing the oscillation field (observationally, this may be say vertical velocity or intensity, but for modelling purposes we shall specialise to another specific choice of Ψ later), the cross-correlation of the signals at positions $\mathbf{x}$ and $\mathbf{x} + \Delta\mathbf{x}$ is

$$\Gamma(\mathbf{x}, \Delta\mathbf{x}, \Delta t) = \int_{-\infty}^{\infty} \Psi(\mathbf{x} + \Delta\mathbf{x}, t + \Delta t)\Psi^*(\mathbf{x}, t)\, dt,$$

(1)

where it is assumed that a wave packet propagates from $\mathbf{x}$ at time t to $\mathbf{x} + \Delta\mathbf{x}$ at $t + \Delta t$. With $\mathbf{x}$ and $\mathbf{x} + \Delta\mathbf{x}$ both on the surface, a time–distance ($\Delta x - \Delta t$) diagram displays a sequence of high-correlation lines, representing respectively one-skip, two-skip, etc. ray travel paths. The theoretical foundations of time–distance helioseismology are set out in D'Silva (1996a; 1996b; see also D'Silva 1994) and D'Silva & Duvall (1995), though it is useful to bear in mind that the observations and the process of forming the cross-correlations and the time–distance diagram is completely independent of ray theory. It is at the level of interpretation and inversion that the ray formalism is introduced as a convenient method of extracting information from the data. An interesting comparison

(independent of ray theory) of the time–distance method with the frequency–wavenumber modal description in local helioseismology is drawn by Bogdan, Braun & Lites (1998).

Most commonly, the observed and analysed oscillations are part of the 'bath' of normal modes continually ringing in their own cavities in the solar interior. In this paper however, we are in part concerned with rays emanating from a compact object (emitted or scattered), and which have not yet bounced between their upper and lower turning points sufficiently often (if at all) for normal modes to be set up. In this case, expansion in terms of normal modes is less appropriate. Specifically, we are concerned with the problem of localising a subsurface emitter or scatterer using observable surface oscillations. It is therefore crucial to derive accurate ray paths. Even given a mature spectrum of normal modes, localisation is a concern. Bogdan (1997) has shown how the rays employed in time–distance helioseismology can be synthesised from a finite collection of p-modes. However, he finds that localisation is very far from perfect because of the dearth of high radial order modes in the solar oscillation power spectrum. It is therefore open to question whether mapping compact subsurface features with high spatial accuracy is achievable with this technique.

Putting these concerns to one side for the moment, a time–distance method known as helioseismic tomography is designed to measure and localise travel time variations along ray paths (Duvall et al. 1996), specifically those passing under and around sunspots. However, the speed of wave packet propagation is well-recognised as depending on a combination of local sound speed, acoustic cut-off frequency, magnetic field, and any flow fields present. To some extent, these can be deconvolved by examining different rays and different propagation directions (Kosovichev & Duvall 1997). However, magnetic effects in particular are treated only crudely as yet, taking account of just the fast magneto-acoustic wave. In reality an incident p- or f-mode couples to a combination of fast and slow magneto-acoustic-gravity modes in a very complicated way (Cally & Bogdan 1993; Cally, Bogdan & Zweibel 1994; Bogdan & Cally 1997; Cally & Bogdan 1997; Cally 2000),[1] and these are not fully accounted for in the ray description (see also D'Silva 1994, where Snell's law is applied to rays incident on magnetic interfaces).

1.2 Acoustic Holography

Another related recent method is acoustic holography, developed for application to the Sun by Lindsey & Braun (1997; 1998; 1999; 2000) and Braun & Lindsey (2000a; 2000b). It is assumed that the solar surface acoustic field $\psi(\mathbf{r}, t) = \Psi(\mathbf{r} + z_s \hat{\mathbf{e}}_z, t)$ has been observed in some annulus (the pupil) of inner radius a and outer radius b at the surface z_s over some period of time. Here $\mathbf{r}$ denotes the

---

[1]It is interesting though that some aspects of this complex process can be modelled as purely a surface effect (Barnes & Cally 2000).

horizontal coordinates only. In the space–time perspective, the 'acoustic egression' H_+ and 'acoustic ingression' H_- are defined by

$$H_{\pm}(\mathbf{r}, z, t) = \iint_{a < |\mathbf{r} - \mathbf{r}'| < b} G_{\pm}(|\mathbf{r} - \mathbf{r}'|, z, t - t') \times \psi(\mathbf{r}', t') \, d^2\mathbf{r}' \, dt', \quad (2)$$

where G_+ is a Green's function expressing how a single transient point disturbance at $(\mathbf{r}', z_s, t')$ propagates to $(\mathbf{r}, z, t)$, and $G_-(|\mathbf{r} - \mathbf{r}'|, z, t - t') = G_+(|\mathbf{r} - \mathbf{r}'|, z, t' - t)$ is its time reverse. Since both the spatial and the temporal quadratures here are convolution integrals, Fourier transforms reduce them to products, with consequent computational advantages. In particular, the wavenumber–frequency version of (2) is

$$\hat{H}_{\pm}(\mathbf{k}_\perp, z, \nu) = \hat{G}_{\pm}(|\mathbf{k}_\perp|, z, \nu) \, \hat{\psi}(\mathbf{k}_\perp, \nu) \quad (3)$$

which is useful if the plane-parallel projection is appropriate, and the space–frequency version is

$$\check{H}_{\pm}(\mathbf{r}, z, \nu) = \int_{a < |\mathbf{r} - \mathbf{r}'| < b} \check{G}_{\pm}(|\mathbf{r} - \mathbf{r}'|, z, \nu) \check{\psi}(\mathbf{r}', \nu) \, d^2\mathbf{r}', \quad (4)$$

which may be used for larger pupils, or when dispersion is important.

The time taken for a wavefront emanating from a point acoustic source at depth z to reach a surface point horizontal distance r away is assumed to be given by

$$T(r, z) = \min_{\Lambda} \int_{\Lambda} \frac{ds}{c} \quad (5)$$

where Λ represents a path joining these two points, c is the sound speed, and ds an element of arc length. This is Fermat's principle, that the true ray path between fixed points minimises travel time. However, this is only approximately true in the Sun, a point revisited in Section 2. Lindsey & Braun (1997) next write

$$G_+(|\mathbf{r} - \mathbf{r}'|, z, t - t') = \delta[t - t' - T(|\mathbf{r} - \mathbf{r}'|, z)] f(|\mathbf{r} - \mathbf{r}'|, z). \quad (6)$$

Here $f(r, z)$ represents the pulse amplitude, which is determined from the condition that wave energy flux is conserved. If we assume that we have a satisfactory mean model for the sound speed as a function of depth, the egression and ingression can be calculated numerically at any subsurface point. The crudest measure of a subsurface acoustic field is provided by the 'acoustic power'

$$P(\mathbf{r}, z) = \int_{\Delta t} |H_+(\mathbf{r}, z, t)|^2 \, dt, \quad (7)$$

where Δt is a considerable time containing many wave periods. Phase sensitive holography uses the temporal correlation of the egression and the ingression

$$C(\mathbf{r}, z, \tau) = \int_{\Delta t} H_-(\mathbf{r}, z, t) \, H_+(\mathbf{r}, z, t + \tau) \, dt, \quad (8)$$
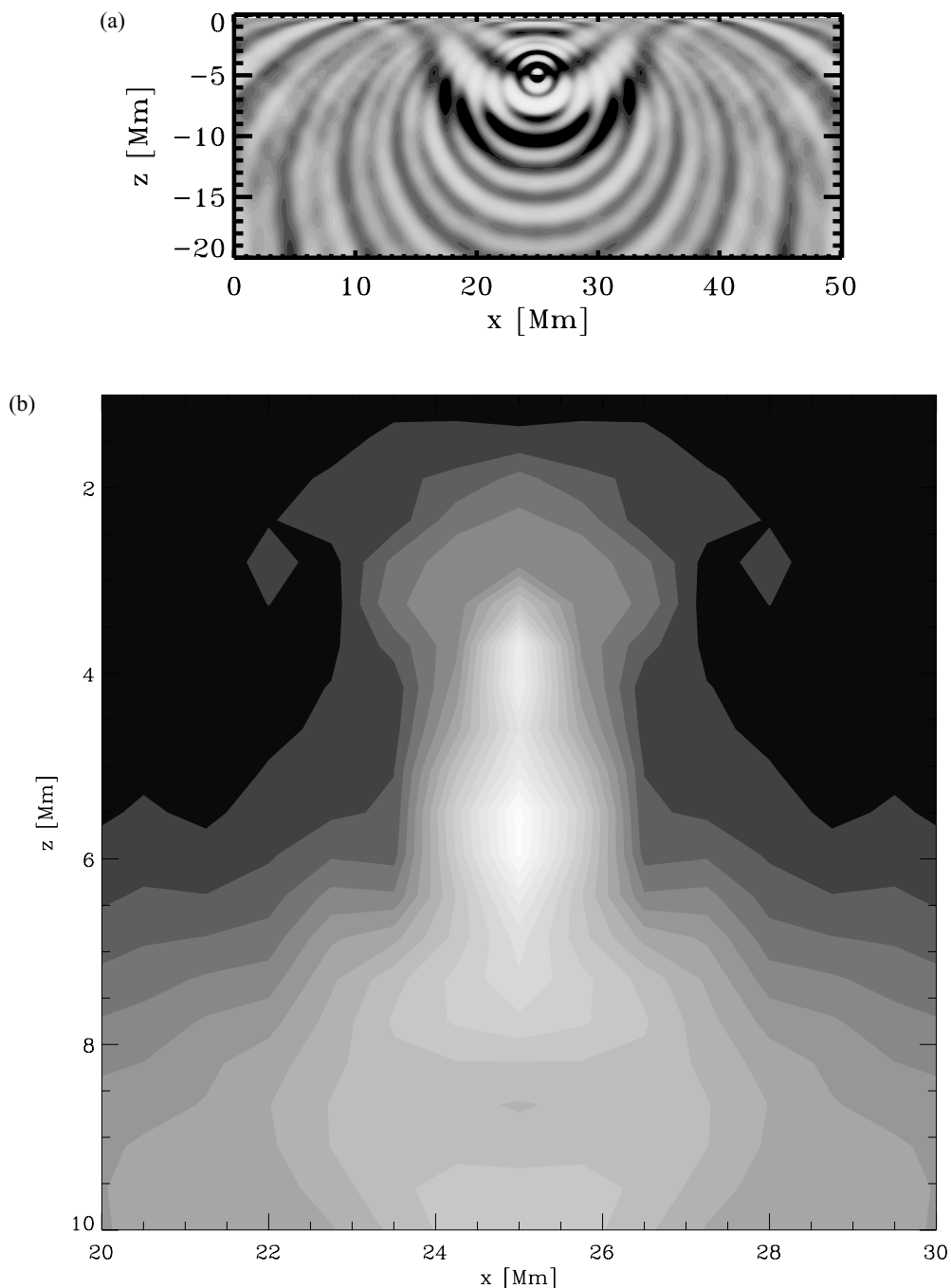
Figure 1   (a) Density perturbation determined numerically for a truncated 2D isentropic $m = 1.5$ polytrope containing a Gaussian source region (horizontal position $x = 25$ Mm, depth $z = 5$ Mm, standard deviation $\sigma = 0.3$ Mm) vibrating simultaneously with ten superimposed frequencies between 1 mHz and 20 mHz. (b) Acoustic power (cf. equation (7)) determined numerically from surface oscillations of the model of Figure (a).

from which travel times may be determined. Horizontal flow maps may be generated in this way.

As an experiment, we calculated the acoustic field due to a compact acoustic source in a polytropic atmosphere, generated using the 2D finite difference code of Cally (2000). The resulting surface oscillations were then applied as described above to determine the subsurface acoustic power. Figure 1 displays both the actual acoustic field and the holographic power image. Clearly, the method is broadly successful at detecting the source, but does not localise it very well.

Now, the formula for the egression is built upon the Green's function for the most basic wave equation (see equation [9] below). It is therefore 'aware' of the underlying atmosphere only through the sound speed in equation (5), and so is clearly incapable of taking account of dispersion associated with the cut-off or Brunt-Väisälä frequencies. In reality, ray paths and travel times are

frequency dependent. In the next section we set up the theory for treating dispersive solar oscillations properly, and apply it to both a simple polytrope and a realistic solar model. It is hoped that, combined with the space–frequency formulation, this will prove useful in further developing acoustic holography so as to produce higher resolution images.

2 Ray Paths for Acoustic Waves in a General Atmosphere

The ray formalism forms the prime descriptive context of ocean acoustics (Munk, Worcester & Wunsch 1995), and a considerable body of theory has been developed in that field. In the oceans, the effect of gravity and density gradients is negligible for frequencies above 1 Hz (see Brekhovskikh & Lysanov 1982, §2.1), and so the wave equation in its most basic form suffices:

$$\frac{\partial^2 \Psi}{\partial t^2} = c^2 \nabla^2 \Psi, \qquad (9)$$

where t is time, c is the sound speed, and Ψ is some measure of the acoustic field, e.g. the pressure perturbation, or the velocity potential. For this system, Fermat's principle applies, i.e. ray paths are associated with an extremum in travel time.

Introducing the dependent variable

$$\Psi(\mathbf{x}, t) = \rho^{1/2} c^2 \nabla \cdot \boldsymbol{\xi}, \qquad (10)$$

where $\boldsymbol{\xi}$ is the displacement and ρ is the equilibrium density, and otherwise following the method of Lamb (1932), the fundamental equation governing acoustic disturbances in an atmosphere such as the Sun can be written as

$$\left(\nabla^2 - \frac{\omega_c^2}{c^2} - \frac{1}{c^2}\frac{\partial^2}{\partial t^2}\right)\frac{\partial^2 \Psi}{\partial t^2} = -N^2 \nabla_\perp^2 \Psi, \qquad (11)$$

where $\nabla_\perp^2$ is the horizontal part of the Laplacian, $N^2 = g/H_\rho - g^2/c^2$ is the squared Brunt-Väisälä frequency, g is the gravitational acceleration, and

$$\omega_c^2 = \frac{c^2}{4H_\rho^2}\left(1 - 2H_\rho'\right) \qquad (12)$$

is the square of the acoustic cut-off frequency, with $H_\rho(z)$ the density scale height, and $H_\rho' = dH_\rho/dz$. Since we are interested in local features, we work in cartesian coordinates, and assume that each of ρ, N, ω_c and c is a function of vertical coordinate z alone. In the high frequency limit, equation (11) reduces to the simple wave equation (9). For arbitrary frequencies, however, a more general approach must be taken. Following Weinberg (1962) and Bogdan (1997), we look for a solution of the form

$$\Psi(\mathbf{x}, t) = \int \int_{-\infty}^{\infty} \psi_\sigma(\mathbf{x}, \omega)\, e^{i S_\sigma(\mathbf{x}, \omega) - i\omega t}\, d\omega\, d\sigma, \quad (13)$$

where σ is used loosely to represent particular ray paths. For the most part, we shall be concerned with monochromatic radiation, where the ω dependence of ψ has a delta-function form, propagating along one ray path. We shall therefore discard the subscript σ on ψ and S and their explicit ω dependence from now on. The ray-theoretic analysis assumes the amplitude ψ to be slowly varying in the sense that $\ln \psi$ changes slowly compared to S along ray paths.

There are two different types of ray path considered in the literature. One is associated with the *phase* velocity, whilst the other represents the locus of a wave packet as it propagates at the *group* velocity. For example, propagation of the cross-correlation function $\Gamma(\mathbf{x}, \Delta\mathbf{x}, \Delta t)$, which is at the basis of time–distance helioseismology, is related to both descriptions: its envelope peak moves along the group velocity paths, and its phase peaks follow the phase velocity rays (D'Silva 1996b). Kosovichev and Duvall (1997; see also Kosovichev, Duvall & Scherrer 2000) show how both group and phase angular speeds may be derived simultaneously from fits to observational data (see also Chou & Duvall 2000). It is the *group velocity* ray paths which concern us in this paper. However, it should be borne in mind that the formation of stigmatic optical images in holography is dependent on interference based on phase coherence rather than wave-packet timing (we are indebted to Charles Lindsey for bringing this to our attention). Nevertheless, the phase S is also derivable from the 'group velocity' approach (equation [21] and Figure 5 below), and there would not appear to be any disadvantage to this formalism.

Although the ray equations have been set out many times before (e.g. D'Silva 1996a), we adopt a slightly different formalism, and present the analysis in detail in the interests of clarity. Beginning with the full wave equation (11), and substituting (13) into (11), we have

$$\left[\frac{\omega^2 - \omega_c^2}{c^2} + i\left(\nabla^2 S - \frac{N^2}{\omega^2}\nabla_\perp^2 S\right) + \left(|\nabla S|^2 - \frac{N^2}{\omega^2}|\nabla S_\perp|^2\right)\right]\psi$$
$$= -2i\left(\nabla S - \frac{N^2}{\omega^2}\nabla_\perp S\right)\cdot\nabla\psi - \left(\nabla^2\psi - \frac{N^2}{\omega^2}\nabla_\perp^2\psi\right).$$

$$(14)$$

The wavevector is defined by

$$\mathbf{k}(\mathbf{x}) = \nabla S(\mathbf{x}), \qquad (15)$$

with $\mathbf{k}_\perp$ representing the horizontal part of $\mathbf{k}$, and $k \equiv |\mathbf{k}|$. Then, to zeroth order (i.e. ignoring the spatial dependence of ψ and $\mathbf{k}$), the right hand side and the middle term on the left hand side vanish, and a solution is clearly apparent:

$$D_0 \equiv k^2 - \frac{N^2}{\omega^2}k_\perp^2 - \frac{\omega^2 - \omega_c^2}{c^2} = 0. \qquad (16)$$

This is effectively the dispersion relation of Deubner & Gough (1984) equation (2.3), widely used in ray theoretic treatments of solar oscillations (e.g. D'Silva 1996a; D'Silva & Duvall 1995).

Equation (16) partially specifies $\mathbf{k}$. To complete its construction, the standard technique is to define a family of

ray paths given by

$$\frac{d\mathbf{x}}{d\tau} = \frac{\partial D_0}{\partial \mathbf{k}}, \tag{17}$$

$$\frac{d\mathbf{k}}{d\tau} = -\frac{\partial D_0}{\partial \mathbf{x}}, \tag{18}$$

$$\frac{dt}{d\tau} = -\frac{\partial D_0}{\partial \omega}, \tag{19}$$

$$\frac{d\omega}{d\tau} = \frac{\partial D_0}{\partial t}, \tag{20}$$

where τ parametrises the progress of a disturbance along the ray path. Clearly, since D_0 is independent of horizontal position, $k_\perp$ remains constant along a ray. However, the vertical component k_z evolves due to the z dependence of N, c, and ω_c. Furthermore, for a time independent medium, where $\partial D_0/\partial t = 0$, the frequency ω is also invariant along the path. The phase function S evolves according to

$$\frac{dS}{d\tau} = \mathbf{k} \cdot \frac{d\mathbf{x}}{d\tau}, \tag{21}$$

which is easily shown to satisfy (15). For the wave equation in question here, this is equivalent to

$$\frac{dS}{dt} = \omega^3 \frac{\omega^2 - \omega_c^2}{\omega^4 - N^2 c^2 k_\perp^2}, \tag{22}$$

showing how the temporal evolution of phase depends on the cut-off and Brunt-Väisälä frequencies. We note in particular that the simple formula $S = \omega t$ is *not* correct when $\omega_c \neq 0$. This implies that Fermat's principle does not apply.[2]

The function f appearing in the holography Green's function (6) may be identified with the slowly varying amplitude ψ. This is determined in the approximation where terms involving second spatial derivatives of the amplitude are neglected, but first derivatives are retained, from

$$\frac{d\ln\psi}{d\tau} + \frac{1}{2}\nabla \cdot \frac{d\mathbf{x}}{d\tau} = 0. \tag{23}$$

Cartesian and cylindrical geometries may be accommodated neatly if we define

$$\tilde{\psi} = \begin{cases} \psi, & \text{2D cartesian coordinates;} \\ r^{1/2}\psi, & \text{cylindrical coordinates,} \end{cases} \tag{24}$$

where r is the cylindrical radial (horizontal) coordinate. Equation (23) then becomes

$$\frac{d\ln\tilde{\psi}}{d\tau} + \left(1 - \frac{N^2}{\omega^2}\right)\frac{\partial k_\perp}{\partial r} + \frac{\partial k_z}{\partial z} = 0, \tag{25}$$

where r represents either the cartesian or cylindrical horizontal distance. In the latter case, it is assumed that the ray is emanating from $r = 0$. The factor of $r^{1/2}$ in the definition of $\tilde{\psi}$ simply accounts for geometric attenuation in cylindrical geometry. For emission from a point source,

[2]It can be shown (Weinberg 1962) that Fermat's principle applies for any system where D_0 is a homogeneous function of $\mathbf{k}$ and ω.

either 2D cartesian or 3D cylindrical, it is easily shown that, at 'time' τ,

$$\tilde{\psi} \sim \text{constant} \times \tau^{-1/2} \quad \text{as } \tau \to 0^+,$$

and hence $r^{1/2}\tilde{\psi} = O(1)$ in that limit, as we would expect from energy conservation considerations.

Our primary concern in this paper is with the application of Fermat's principle to determining both ray paths and travel times. As we have seen, this is at least formally inappropriate for solar models. Nevertheless, Fermat's principle is widely applied in holography. Strangely, it also seems to be used in time–distance studies where ω_c is retained. For example, Kosovichev & Duvall (1997), equation (12), identify the travel time variations due to underlying flow and magnetic fields (which they treat as perturbations to a background state) as $\delta t = \omega^{-1}\int_\Gamma \delta\mathbf{k} \cdot d\mathbf{x}$, despite including the cut-off frequency in their dispersion relation. This is clearly not correct. We shall now investigate the errors which may be introduced by adopting Fermat's principle.

2.1 A Polytropic Atmosphere

In this section, we briefly apply ray theory to an isentropic, plane-parallel, polytropic atmosphere with polytrope index m. A more detailed exposition may be found in Price (2000). In our model, the Brunt-Väisälä frequency vanishes, and equation (11) reduces to

$$\left[\nabla^2 - \frac{m(m+2)}{4z^2} + \frac{m\omega^2}{gz}\right]\psi = 0, \tag{26}$$

where g is the acceleration due to gravity. Equations (17) and (18) can be solved analytically to give the following expressions for a ray path launched horizontally from its lower turning point:

$$k_\perp z = -\frac{m\omega^2}{2k_\perp g} - \left[\left(\frac{m\omega^2}{2k_\perp g}\right)^2 - \frac{m(m+2)}{4}\right]^{1/2}$$
$$\times \cos\left[\frac{gk_\perp}{m\omega^2}\omega t\right] \tag{27}$$

$$k_\perp x = \frac{\omega}{2}t - \left[\left(\frac{m\omega^2}{2k_\perp g}\right)^2 - \frac{m(m+2)}{4}\right]^{1/2}\sin\left[\frac{gk_\perp}{m\omega^2}\omega t\right] \tag{28}$$

where $k_\perp$ is the (constant) horizontal wavenumber, and $x = 0$ at time $t = 0$. In the limit

$$\omega^4 \gg \frac{k_\perp^2 g^2 (m+2)}{m} \tag{29}$$

these ray paths match those derived by minimising the travel time between two points. For the Sun, where $g_\odot = 274\,\text{m s}^{-2}$ and $m \approx 1.5$, we may reexpress this in terms of the horizontal skip distance, $d = \pi m\omega^2/k_\perp^2 g$, as

$$\left(\frac{\nu}{1\,\text{mHz}}\right)^2 \left(\frac{d}{30\,\text{Mm}}\right) \gg 1. \tag{30}$$
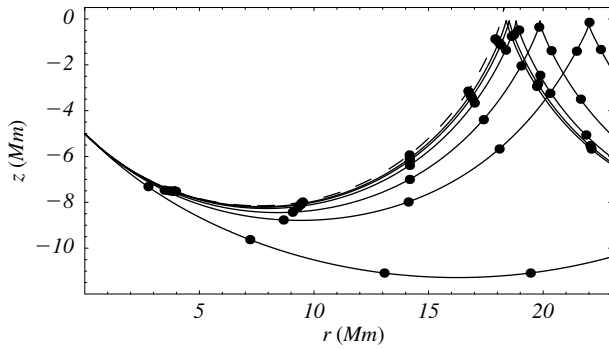
Figure 2 Ray paths for waves in a GONG model atmosphere. The dashed line gives the high frequency limit (actually 100 mHz is used here), while the solid lines are ray paths for frequencies of 2, 3, 4, 6, 8, and 10 mHz (the solid lines, lowest turning depth to highest). The dots on each path are three minutes apart, and indicate propagation speed. Note that even though the 10 mHz path is quite similar to the high frequency limit at depths of order 1 Mm or greater, the behavior at the surface is quite different. Waves with frequencies less than about 10 mHz are reflected by the behaviour of the cut-off frequency near the surface (see Figure 3), while higher frequencies propagate all the way to $z = 0$ and beyond.

The oscillations of most interest for probing sunspots and active regions typically have frequencies of a few milli-Hertz, and skip distances in the range 15–45 Mm (see e.g. Lindsey & Braun 1999), putting them in a regime where differences from the minimised travel time ray paths are potentially significant.

2.2 The Real Sun

Of course, the real Sun is not a polytrope. However, considering a more realistic model of the solar interior does not greatly change things. The most direct way to display dispersion is to launch a multichromatic ray packet in a single direction and observe the different frequency components separating. In Figure 2, we show ray paths calculated numerically from equations (17) and (18) in a GONG solar model[3] fgong.15bi.d.15, which uses OPAL opacities, the Livermore equation of state, and He and Z diffusion. We start the rays from a depth of 5 Mm, at an angle of 45° below the horizontal, for a range of frequencies between 2 mHz and 10 mHz, plus the high frequency limit. At depths greater than about 1 Mm, the ray paths are qualitatively similar, with the deviations from the high frequency limit getting progressively larger as the frequency decreases. At 10 mHz the deviations are not large, but become quite significant by 4 mHz. This should come as no surprise, since the Sun's polytropic index changes slowly at depths greater than about 1 Mm, so the results of the preceding subsection apply. In this case, we are showing waves with horizontal skip distances of order 30 Mm, so we expect that the term dependent upon the cut-off frequency will only be negligible for waves with frequencies much greater than about a milliHertz.

Above a depth of about a megametre, the Sun is no longer well approximated by a polytrope, so the results of
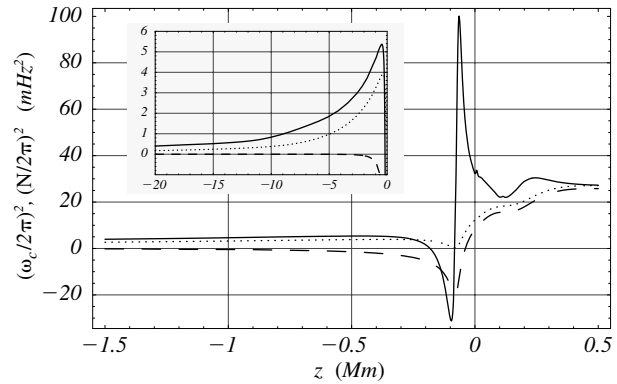
---

[3]Available from http://www.obs.aau.dk/~jcd/adipack.n/

Figure 3 The square of the cut-off frequency (solid line) and the Brunt-Väisälä frequency (dashed line) as a function of depth in a GONG model atmosphere. At depths greater than a few hundred kilometres, the Brunt-Väisälä frequency is negligible even for waves with frequencies of a few milliHertz, while the cut-off frequency makes a significant difference for waves with frequencies of a few milliHertz, but has little impact on waves with frequencies above about 10 mHz. However, even waves with frequencies up to about 10 mHz will be reflected off the spike in the cut-off frequency at $z \approx -100$ km, never reaching $z = 0$ in a ray theoretic treatment. The dotted curve represents $\tilde{\omega}_c = c/2H_\rho$, the 'isothermal' acoustic cut-off frequency. Inset: same, though extending from depth -20 Mm to -0.1 Mm.

the previous subsection are not applicable. The reason that none of the ray paths except the high frequency limit reach the surface has to do with the behaviour of the cut-off frequency and the Brunt-Väisälä frequency just below $z = 0$. Figure 3 shows the squares of both frequencies plotted as a function of depth. It is only within the first few hundreds of kilometres below the surface that either of the frequencies becomes significant in comparison with a frequency of a few milliHertz. The cause of the abrupt changes in the frequencies at $z \approx -100$ km is a change in the ionisation state of hydrogen. What this means for acoustic waves is that those with frequencies less than about 10 mHz will be partially reflected at this depth, and partially transmitted via tunnelling through to the region above, in which they can continue to propagate. However, classical ray theory has no way of dealing with this, and so theoretically rays are completely reflected at this depth. This is very important as observations may well be made in regions which ray theory would suggest no rays have reached. Even waves with frequencies slightly above 10 mHz, which propagate freely through this region, will have theoretical ray paths significantly different from the high frequency limit. However, in reality it is known that the solar surface is largely transparent to rays above about 5 mHz, indicating that they successfully tunnel through the ω_c spike. (Another way of looking at this is that the WKB approximation upon which ray theory is based breaks down in regions of high spatial gradients, and should be supplemented by proper matching procedures; see e.g. Bender & Orszag 1978.) This may be crudely accounted for by simply arbitrarily removing the spike. One way of achieving this is to replace the acoustic cut-off frequency given by (12) by the 'isothermal' value $\tilde{\omega}_c = c/2H_\rho$ (Jefferies et al. 1994), depicted in Figure 3 by the dotted curve. We do not implement this.

The frequency dependence of the amplitude, at the level of approximation adopted in this paper, is generally weaker than that of the ray paths for disturbance with frequencies of a few milliHertz. In Figure 4, we show the amplitude as a function of horizontal distance from a point source for the 4 mHz and high frequency limit cases of the rays shown in Figure 2. Along most of the ray paths,
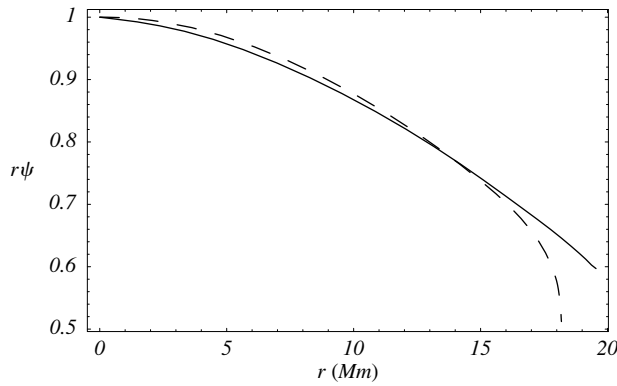

Figure 4 The slowly varying amplitude, ψ, times the horizontal distance, r, as a function of horizontal distance for the 4 mHz (solid line) and high frequency limit (dashed line) rays shown in Figure 2. Compared with the changes in the ray paths, the amplitude shows a weaker frequency dependence except near the upper turning point ($r \approx 18$ Mm).

the deviation from the high frequency limit is fairly small compared with that of the ray path. However, some significant differences do appear near the upper turning point, where ray theory as described here breaks down.

As mentioned earlier, the phase S is of prime importance in holography. This is displayed as a function of both r and z in Figure 5, again for 4 mHz. In this case, comparison is made not with the high frequency limit, but with an atmosphere having the same sound speed profile, but zero cut-off and Brunt-Väisälä frequencies. It is seen that the difference in phase at the upper turning point (end of the full curves) is quite small, but that their horizontal positions are significantly different.

Another measure of dispersion is provided by the primary tool of time–distance helioseismology, the time–distance diagram. In Figure 6 we show how this varies with frequencies ranging from 2 mHz to 6 mHz. Clearly, the deviations from the 'infinite frequency' approximations (Figure 7) are substantial, especially at low frequencies. Indeed, variations of one to several minutes are large in comparison to typical perturbations encountered in studies of sub-surface temperature enhancements, flows, and magnetic fields (e.g. around 20 seconds as reported by Duvall et al. 1996). This raises concerns about interpretation. For example, Duvall et al. (1996) measure travel times between a surface point and a surrounding
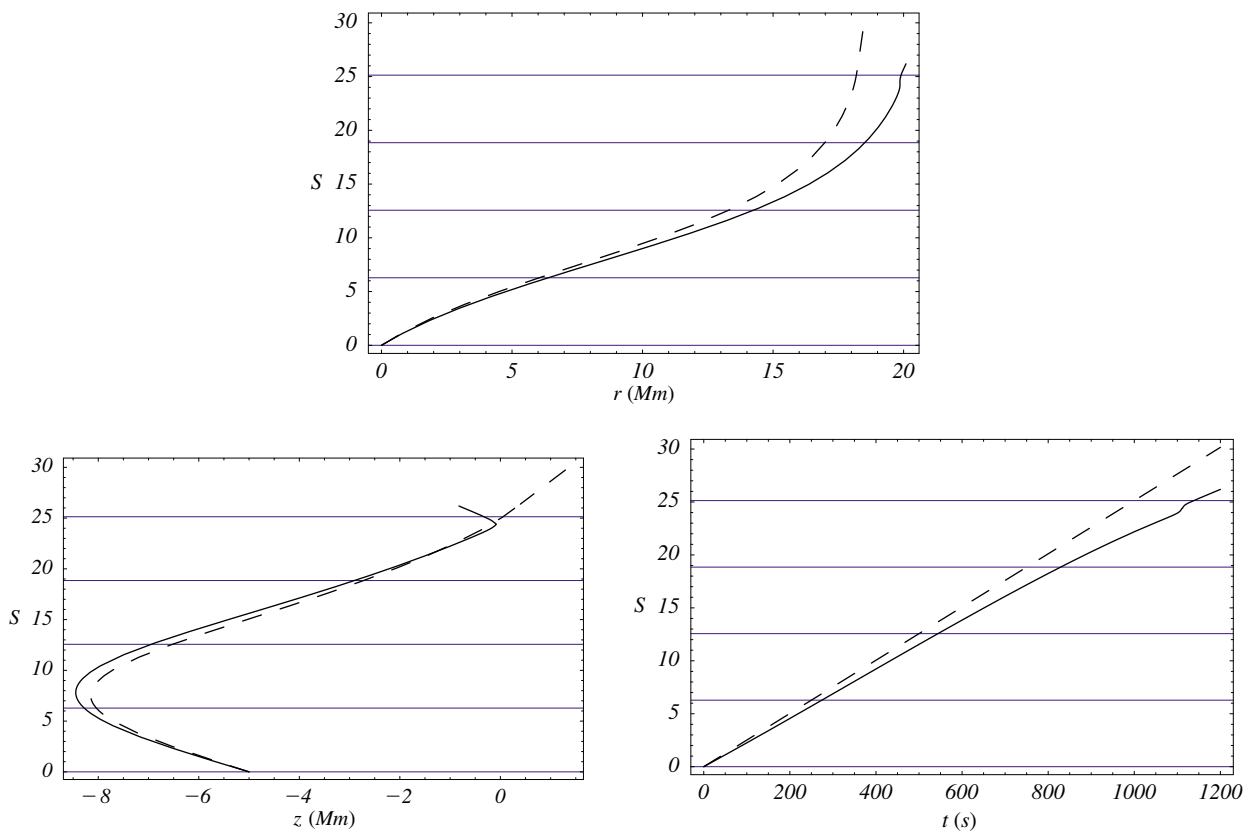

Figure 5 The phase S as a function of horizontal distance (top frame), depth (lower left), and time (lower right) for the 4 mHz case in Figure 2, with (solid line) and without (dashed line) the cut-off and Brunt-Väisälä frequencies. The integration time is the same for both models. The horizontal grid lines represent multiples of 2π.
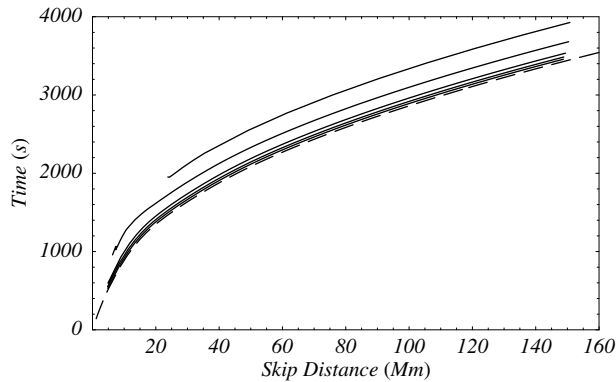
Figure 6 The single skip time–distance curves of the solar model for a range of frequencies: 2 mHz (top curve), 3 mHz, 4 mHz, 5 mHz, 6 mHz (bottom full curve). These are the times and horizontal distances between successive skips, not successive crossings of a set 'surface' z_s. However, due to the steepness of the cut-off spike displayed in Figure 3, this turning point lies between -0.08 and $-0.07\,\mathrm{Mm}$ in each case, with only a very weak dependence on ω and $k_\perp$. The dashed curve corresponds to the 'infinite frequency' case in which ω_c and N are set to zero. However, since this ray path does not 'skip', because of the finite height of the cut-off peak, the times and distances have been chosen to represent separations between two points on the 'surface' $z = 0$.
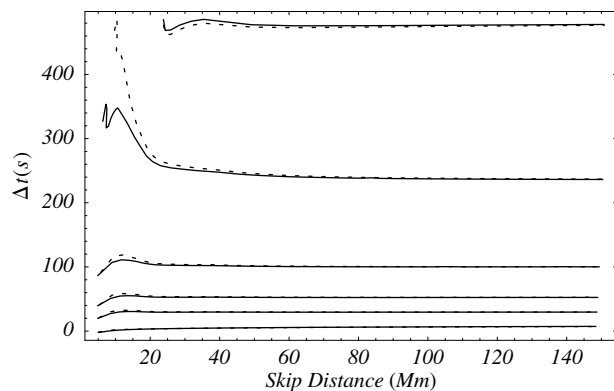

Figure 7 The delay Δt between the single skip times at frequencies 2 mHz (top full curve), 3 mHz, 4 mHz, 5 mHz, 6 mHz, and 10 mHz (bottom full curve) compared to the 'infinite frequency' skip time (dashed curve in Figure 6). The dotted curves represent single skip delays where the Brunt-Väisälä frequency N is set to zero throughout, but ω_c is left unchanged.

annulus, and filter out flows by averaging ingoing and outgoing rays. The remaining differences with average travel times over the surface were attributed to local wave speed enhancements, in particular, sound speed (temperature) inhomogeneities. However, our results show that local variations in acoustic cut-off and Brunt-Väisälä frequencies may also be relevant, as these too greatly affect travel time. The relative importance of sound speed versus ω_c and N variations may be estimated by utilising a range of different frequencies. Indeed, Jefferies et al. (1994) present an inversion method for ω_c based on travel times. Figure 7 also shows the frequency dependent travel time variation if the Brunt-Väisälä frequency is set to zero. This suggests that N could possibly be probed using short-skip 3 mHz rays.

3 Conclusions

While holography has a great deal of potential to reveal subsurface structures in the Sun, care must be taken in applying it. For the frequency regime of most interest, the ray paths must be determined from a formulation which includes the effects of the cut-off frequency and the Brunt-Väisälä frequency. At shallow depths in particular (the first few hundreds of kilometres below the surface), these additional terms can change the ray paths for waves with frequencies less than about 5 mHz quite significantly. In a model solar atmosphere, including these terms also leads to the reflection of rays at a depth of about one hundred kilometres below the surface, suggesting that even a classical ray treatment involving the frequency dependent terms will not adequately model these layers. In addition to modifying the ray paths, these extra terms also affect the amplitude and phase of an acoustic wave, although this is usually a smaller effect than the changes in the paths themselves. As discussed by Bogdan (1997) though, it is far from clear that a single ray can adequately represent a wave packet for low frequency waves. Instead, ray bundles must be constructed. Despite these limitations, we feel that its already considerable successes show it to be an extremely valuable tool.

References

Barnes, G., & Cally, P. S. 2000, Sol. Phys., 193, 373
Bender, C. M., & Orszag, S. A. 1978, Advanced Mathematical Methods for Scientists and Engineers (New York: McGraw-Hill)
Bogdan, T. J. 1997, ApJ, 477, 475
Bogdan, T. J., Braun, D. C., & Lites, B. W. 1998, ApJ, 492, 379
Bogdan, T. J., & Cally, P. S. 1997, Proc. R. Soc. London A, 453, 943
Braun, D. C. 1995, ApJ, 451, 859
Braun, D. C., & Lindsey, C. 2000a, Sol. Phys., 192, 285
Braun, D. C., & Lindsey, C. 2000b, Sol. Phys., 192, 307
Brekhovskikh, L., & Lysanov, Yu. 1982, Fundamentals of Ocean Acoustics (Berlin: Springer-Verlag)
Cally, P. S. 2000, Sol. Phys., 192, 395
Cally, P. S., & Bogdan, T. J. 1993, ApJ, 402, 721
Cally, P. S., & Bogdan, T. J. 1997, ApJ, 486, L67
Cally, P. S., Bogdan, T. J., & Zweibel, E. G. 1994, ApJ, 437, 505
Charbonneau, P., Tomczyk, S., Schou, J., & Thompson, M. J. 1998, ApJ, 496, 1015
Chou, D.-Y., & Duvall, T. L. Jr. 2000, ApJ, 533, 568
Christensen-Dalsgaard, J., & Berthomieu, G. 1991, in Solar Interior and Atmosphere, ed. Cox, A. N., Livingston, W. C., & Matthews, M. S., The University of Arizona Press, 401
Christensen-Dalsgaard, J., Gough, D. O., & Thompson, M. J. 1991, ApJ, 378, 413
Christensen-Dalsgaard, J., Duvall, T. L., Gough, D. O., Harvey, J. W., & Rhodes, E. J. 1985, Nature, 315, 378
Deubner, F.-L. 1975, A&A, 44, 371
Deubner, F.-L., & Gough, D. 1984, ARA&A, 22, 593
D'Silva, S. 1994, ApJ, 435, 881
D'Silva, S. 1996a, ApJ, 469, 964
D'Silva, S. 1996b, ApJ, 462, 519
D'Silva, S., & Duvall, T. L. Jr. 1995, ApJ, 438, 454
Duvall, T. L. Jr., Jeffries, S. M., Harvey, J. W., & Pomerantz, M. A. 1993, Nature, 362, 430

Duvall, T. L. Jr., D'Silva, S., Jeffries, S. M., Harvey, J. W., & Schou, J. 1996, Nature, 379, 235

Hill, F., Deubner, F.-L., & Isaak, G. 1991, in Solar Interior and Atmosphere, ed. Cox, A. N., Livingston, W. C., & Matthews, M. S., The University of Arizona Press, 329

Jefferies, S. M., Osaki, Y., Shibahashi, H., Duvall, T. L. Jr., Harvey, J. W., & Pomerantz, M. A. 1994, ApJ, 434, 795

Kosovichev, A. G., & Duvall, T. L. Jr. 1997, in SCORe'96: Solar Convection and Oscillations and their Relationship, ed. Pijpers, F. P., Christensen-Dalsgaard, J., & Rosenthal, C. S., Kluwer, 241

Kosovichev, A. G., Duvall, T. L. Jr., & Scherrer, P. H. 2000, Sol. Phys., 192, 159

Lamb, H. C. 1932, Hydrodynamics, 6th ed., Cambridge University Press

Lindsey, C., & Braun, D. C. 1997, ApJ, 485, 895

Lindsey, C., & Braun, D. C. 1998, ApJ, 509, L129

Lindsey, C., & Braun, D. C. 1999, ApJ, 510, 494

Lindsey, C., & Braun, D. C. 2000, Sol. Phys., 192, 261

Munk, W., Worcester, P., & Wunsch, C. 1995, Ocean Acoustic Tomography, Cambridge University Press, 40

Price, G. H. 2000, Sol. Phys., 192, 211

Unno, W., Osaki, Y., Ando, H., Saio, H., & Shibahashi, H. 1989, Nonradial Oscillations of Stars (University of Tokyo Press)

Weinberg, S. 1962, Phys. Rev., 126, 1899